Coherent control of non-Markovian photon-resonator dynamics

A. F. J. Levi

Department of Physics and Astronomy and Department of Electrical Engineering,
University of Southern California, Los Angeles, California 90089-0484, USA

L. Campos Venuti, T. Albash, and S. Haas

Department of Physics and Astronomy, University of Southern California, Los Angeles, California 90089-0484, USA

We study the unitary time evolution of photons interacting with a dielectric resonator using coherent control pulses. We show that non-Markovianity of transient photon dynamics in the resonator subsystem may be controlled to within a photon-resonator transit time. In general, appropriate use of coherent pulses and choice of spatial subregion may be used to create and control a wide range of non-Markovian transient dynamics in photon-resonator systems.

I. INTRODUCTION

The transient dynamics of photons interacting with a resonator is of both fundamental and practical interest. For example, microcavity resonators have been explored as a means to delay light in classical communication systems [1], and similar ideas have been developed for single photons [2–4] with potential future use in quantum communication protocols. These and other studies exploit a basic property of a resonator subsystem, namely, the ability to store photon energy density and release it at a later time. Since Markovian dynamics may be identified with information flow leaving the system [5], it seems natural to expect that storage of a photon or many photons in a resonator can result in non-Markovian behavior. More precisely, if we consider a finite region of a resonator, energy can both enter and leak out of the designated region depending on the interplay of system parameters and the location of the region itself. It seems natural to expect a high degree of non-Markovianity in such a situation. Furthermore, non-Markovianity may be viewed as a resource for information processing tasks [6]. One is therefore motivated to demonstrate control of photon transient dynamics and hence control of the associated non-Markovianity.

To investigate such non-Markovian effects we study the full time evolution of a Hamiltonian system and concentrate on the dynamics of a subregion obtained by tracing out exactly the remaining degrees of freedom. In a unitary system of finite spatial extent, excitations are reflected indefinitely back and forth from the boundaries, and consequently, any subregion of such a system would always display non-Markovian behavior. The same holds true for a system with discrete energy levels because of the formation of bound states. To avoid these trivial cases, we seek therefore a system with a continuous energy spectrum such that the subsystem can exchange continuous energy with its environment as sketched in Fig. 1(a).

The physics we are interested in exploring may be captured by a single resonator with a refractive index profile as illustrated in Fig. 1(b). The symmetric one-dimensional Fabry-Pérot resonator consists of three spatial regions, A, B, and C, in vacuum separated by two lossless dielectric mirrors, each of refractive index n_r and thickness $L_m = \lambda_0/4n_r$, where λ_0 is the resonant photon wavelength in vacuum. Spatial regions

A and C connect to continuous input and output states at $x = x_A$ and $x = x_C$, respectively. The resonator cavity length is L_B and defines the spatial extent of region B. At the resonant photon wavelength, the complex mirror reflection amplitude is $re^{i\pi} = -r$, and the transmission amplitude is $te^{i\pi/2} = it$. Flux conservation in the lossless system requires $|r|^2 + |t|^2 = 1$. Transmission through each mirror depends weakly on wavelength such that

$$|t|^2 = \frac{1}{1 + \left(\frac{k_1^2 - k_2^2}{2k_1 k_2}\right)^2 \sin^2(k_2 L_m)} \,, \tag{1}$$

where the propagation constant in vacuum is $k_1 = 2\pi/\lambda$ and in the dielectric mirror it is $k_2 = 2\pi n_r/\lambda$.

A single photon may be described by a wave function $\Psi(x,t)$ with the interpretation that $|\Psi(x,t)|^2$ is the photon energy density [7–9]. We choose to use a single-photon wave function description because, as will become apparent, it has the significant advantages in this initial study of both simplicity and ease of interpretation. The unitary dynamics of the photon wave function propagating in the x direction in a lossless dielectric media may be modeled as a phase-coherent integral of linearly polarized basis states $\phi_\omega(x)$ with amplitudes α_ω,

$$\Psi(x,t) = \int \frac{d\omega}{2\pi} \alpha_\omega \phi_\omega(x) e^{-i\omega t} \,, \tag{2}$$

where, as shown in the Appendix, $\phi_\omega(x)$ is a normalized solution of the one-dimensional Helmholtz equation,

$$\frac{d}{dx}\left(\frac{1}{\mu_r(x)}\frac{d}{dx}\phi_\omega(x)\right) + \omega^2 \epsilon_r(x)\epsilon_0 \mu_0 \phi_\omega(x) = 0. \tag{3}$$

The permeability of vacuum μ_0 and permittivity of vacuum ϵ_0 are related to the speed of light in vacuum via $c = 1/\sqrt{\epsilon_0 \mu_0}$. Assuming the lossless dielectric material, the spatial profile may be characterized by piecewise-constant values of relative permeability μ_r and relative permittivity ϵ_r in each region of the domain; the conditions imposed on $\phi_\omega(x)$ at the boundary between regions 1 and 2 at position x_0 are

$$\phi_\omega(x)|_{x=x_0-\delta} = \phi_\omega(x)|_{x=x_0+\delta} \tag{4}$$
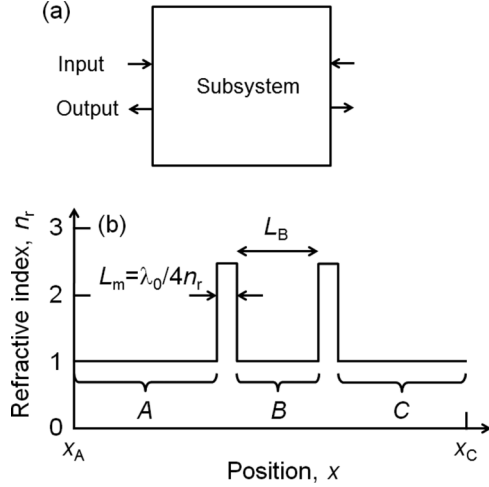
FIG. 1. (a) Sketch of a subsystem with inputs and outputs to continuum states. (b) Symmetric Fabry-Pérot resonator subsystem divided into spatial regions A, B, and C separated by a quarter-wavelength lossless dielectric characterized by refractive index n_r. The resonant wavelength is λ_0.

and

$$\frac{1}{\mu_{r_1}} \frac{d}{dx} \phi_\omega(x) \bigg|_{x=x_0-\delta} = \frac{1}{\mu_{r_2}} \frac{d}{dx} \phi_\omega(x) \bigg|_{x=x_0+\delta} . \tag{5}$$

The refractive index is $n_r = \sqrt{\mu_r}\sqrt{\epsilon_r}$. If we assume that the photon coherence time is longer than any other characteristic time scale, we may simply solve Eq. (3) to completely describe the evolution of the photon. In the thermodynamic limit there are a large number of photons in the system, and Eq. (3) may also be used with the interpretation that the wave function corresponds to the classical electric field [7–9]. This means that our model simultaneously describes a single photon and a classical electromagnetic field.

An efficient and accurate way to solve Eq. (3) for the Fabry-Pérot resonator subsystem coupled to continuous input and output states is to use the propagation matrix method [10,11]. All numerical simulations we present as part of our study use this method.

II. TRANSIENT RESPONSE

We consider the transient response of a rectangular single-photon pulse traveling left to right and incident on the Fabry-Pérot resonator. We smoothen the rectangular pulse with center frequency ω_0 by modulating a sinc function by a cosine in order to reduce the Gibbs phenomenon. In this way a rectangular pulse of duration $2T_0$ (length $2T_0 c$) with rise and fall time $\tau_r = 2\pi/\Delta\omega_r$ may be written as

$$\Psi(x,t) = \int_{|\omega-\omega_0| \leqslant \Delta\omega_r} \frac{d\omega}{2\pi} \left[1 + \cos\left(\frac{\pi(\omega-\omega_0)}{\Delta\omega_r}\right) \right]$$
$$\times \frac{\sin[(\omega-\omega_0)T_0]}{(\omega-\omega_0)T_0} \phi_\omega(x) e^{-i\omega t} . \tag{6}$$

To connect to existing photon technology we choose a cavity with resonant wavelength $\lambda_0 = 1500$ nm and resonant frequency $\omega_0 = 2\pi/\tau_0$, where $\tau_0 = 5$ fs corresponds to a

resonant photon energy of $E_0 = \hbar\omega_0 = 0.827$ eV. The refractive index of the mirrors is chosen to be $n_r = 2.5$, region A has length L_A, region C has length L_C, and, unless stated otherwise, the resonator cavity length is $L_B = 15 \times \lambda_0$. The photon cavity round-trip time is $\tau_{RT} = 2L_B/c = 2\pi/\Delta\omega = 30 \times \tau_0 = 150$ fs, and the resonator quality factor is $Q = 144$, where $\tau_Q = Q/\omega_0 = 114$ fs. Typically, one describes a transient response dominated by the ring-down time constant $\tau_Q = 1/\Gamma$, where the photon energy density of a loaded resonator decays as e^{-t/τ_Q} and in which τ_Q is connected via a Fourier transform to a steady-state Lorentzian energy density spectrum [12,13],

$$S(\omega) = \frac{S_0}{(\omega-\omega_0)^2 + (\Gamma/2)^2} . \tag{7}$$

However, the actual transient dynamics of the system we wish to control is more complex than this description would suggest.

Figure 2(a) shows the calculated space-time photon energy density plot of a rectangular pulse initially moving left to right and incident on the Fabry-Pérot resonator. The presence
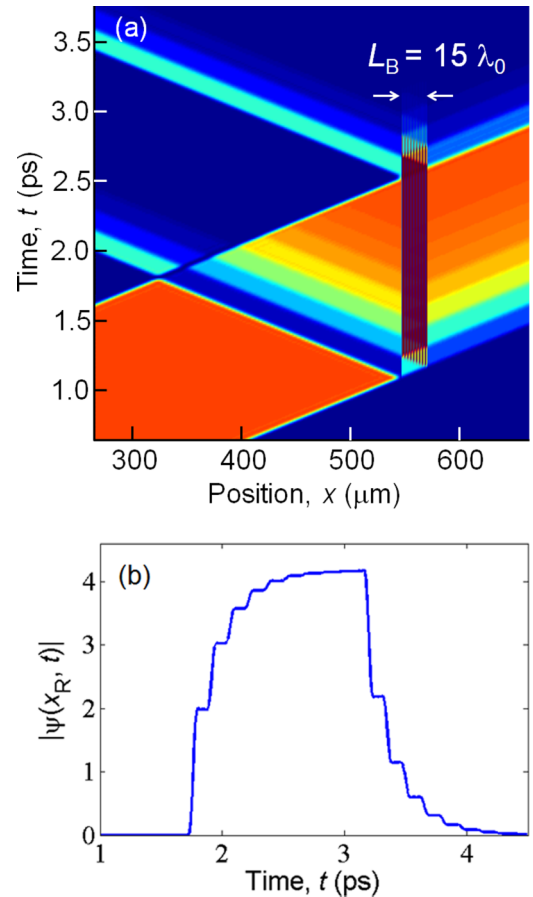

FIG. 2. (Color online) (a) Space-time photon energy density plot of a rectangular pulse incident on a Fabry-Pérot resonator. The resonator is of length L_B (indicated by two arrows). (b) $|\psi(x_R,t)|$ (arbitrary scale) as a function of time detected at position x_R far to the right of the resonator. The field decay constant $2\tau_Q = 229$ fs is modulated by stepwise response at the resonant cavity round-trip time $\tau_{RT} = 30\tau_0 = 150$ fs. Photon pulse parameters are $\hbar\omega_0 = 0.827$ eV, $\hbar\Delta\omega_s = 0.207$ eV, and $T_0\omega_0 = 900$.

of the resonator imparts temporal structure onto reflected and transmitted photon energy density. The reflection at the leading edge and trailing edge of the incident pulse is due to frequency components associated with the pulse transient rise and fall times and the changing energy density in the resonator. Subsequent reflections decay temporally in a stepwise fashion in time steps of duration τ_{RT}. Figure 2(b) shows $|\Psi(x_R,t)|$ calculated as a function of time detected at position x_R far to the right of the resonator. Photon energy density both in the resonator and transmitted to position x_R does not increase (or decay) as a simple exponential; rather, there is a stepwise buildup (or decay) at each resonant cavity photon round-trip time τ_{RT} [14]. With increasing rectangular pulse duration, energy density asymptotically approaches the steady-state value, which, on resonance at frequency ω_0, results in unity transmission and maximum energy density in the resonator. However, our interest is not the steady state; rather, we seek to coherently control the transient photon-resonator interaction using interference effects and in this way control non-Markovianity of the system. The shortest time scale on which we seek to exert control is the photon cavity transit time $\tau_{RT}/2$.

Physical intuition and development of control concepts are best illustrated using a photon pulse whose duration is short compared to the cavity round-trip time, i.e., $2T_0 < \tau_{RT}$. Figure 3(a) shows the space-time photon energy density plot of a short rectangular pulse initially moving left to right and incident on the Fabry-Pérot resonator. Initially, the photon energy density pulse entering the cavity shows no indication of wave character. It is only after reflection from the right mirror that self-interference effects are observed and photon resonances inside the cavity begin to build up. The energy stored in the resonator leaks out as forward and backscattered pulses. The shortest time between forward and backscattered pulses is the photon cavity transit time $\tau_{RT}/2$.

Figure 3(b) illustrates the origin of the ring-down observed in the space-time diagram using space-time *resonant* photon ray tracing of reflected and transmitted amplitudes. The scattered amplitudes at each mirror form a geometric series.

III. COHERENT CONTROL OF TRANSIENT RESPONSE

Coherent control of the transient response illustrated in Fig. 3 may be achieved using photon control pulses. Similar to Eq. (2), the control pulses consist of a coherent integral of basis functions whose amplitudes $\alpha_\omega^{\text{cont}}$ and time delay t_ω^{cont} are control parameters that can be optimized. In the following we avoid the use of formal optimization methods because the geometric series illustrated in Fig. 3(b) suggests a simpler intuitive approach.

First, we consider a single control pulse that is just an attenuated, delayed, and phase-shifted version of the lead pulse. Figure 4(a) is a space-time photon energy density plot showing a lead pulse and control pulse initially moving left to right and incident on the Fabry-Pérot resonator. In this example the control pulse is configured to eliminate ring-down after exactly one photon round-trip time in the cavity. This can be achieved with a control pulse of the same shape that is coherent with the lead pulse, with resonant amplitude $-r^2$ relative to the lead pulse, and delayed by a time τ_{RT}. Figure 4(b) is a space-time
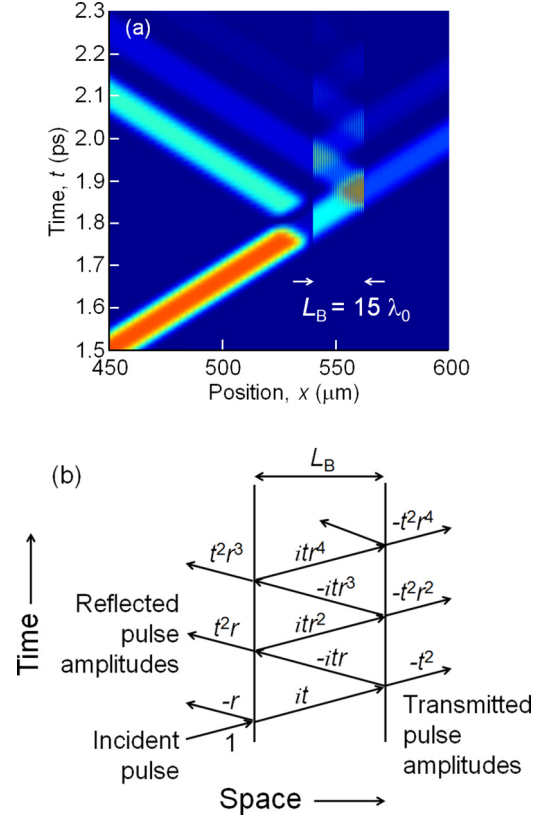

FIG. 3. (Color online) (a) Space-time photon energy density plot of a short rectangular pulse incident on the Fabry-Perot resonator showing ring-down. (b) Space-time resonant photon ray trace illustrating ring-down in the form of multiple transmitted and reflected amplitudes. Photon pulse parameters are $\hbar\omega_0 = 0.827$ eV, $\hbar\Delta\omega_s = 0.207$ eV, and $T_0\omega_0 = 60$.

resonant photon ray trace showing lead and control amplitudes configured to eliminate ring-down.

To highlight the difference in the time domain between uncontrolled ring-down of the resonator and precise control, Fig. 5 shows the transmitted pulse train for the two situations illustrated in Figs. 3 and 4. Transmitted photon energy density as a function of time for the uncontrolled case [Fig. 5(a)] consists of a series of pulses whose peaks occur at equally spaced time intervals τ_{RT} and whose peak value decreases exponentially as e^{-t/τ_Q}. For the controlled case [Fig. 5(b)] a coherent control pulse is used to ensure that there is just one transmitted photon energy density pulse.

A coherent control pulse with amplitude $-r^{2N}$ injected at the Nth photon round-trip may be used together with an *integrating* detector to evaluate a finite geometric sum. Figure 6(a) illustrates this for the case $N = 3$. An integrating photon energy detector at the output measures this geometric sum as

$$\left| \sum_{n=0}^{N-1} ax^n \right|^2 = \left| a\frac{1-x^N}{1-x} \right|^2, \tag{8}$$

where, on resonance, $x = r^2$ and $a = t^2$. The sum in Eq. (8) is guaranteed to converge in the limit $N \to \infty$ because $|r| < 1$.

Figure 6(b) illustrates that the finite geometric series in Eq. (8) with $|x| > 1$ may also be created by using multiple

FIG. 6. (Color online) (a) Space-time resonant photon ray trace showing incident lead and control amplitudes configured to perform a finite geometric sum. (b) Space-time resonant photon ray trace showing incident lead photon and control amplitudes configured to create a finite divergent geometric series.
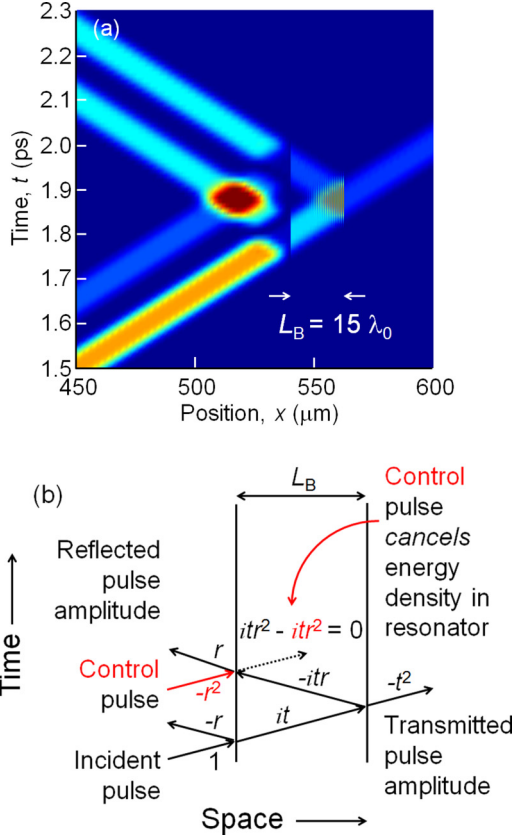

FIG. 4. (Color online) (a) Space-time photon energy density plot showing lead and control pulses. The control pulse eliminates ring-down by removing all photon energy density in the cavity after exactly one round-trip time τ_{RT}. There is just one transmitted photon pulse. (b) Space-time resonant photon ray trace showing lead and control amplitudes configured to eliminate ring-down. Photon pulse parameters are $\hbar\omega_0 = 0.827$ eV, $\hbar\Delta\omega_s = 0.207$ eV, and $T_0\omega_0 = 60$.

forward- and reverse-propagating control pulses. In this particular example coherent photon control pulses are used to *confine* photon energy density in the resonator. The photon energy density in the resonator increases according to Eq. (8) because $|r| < 1$ and so $|x| = |e^{i\phi}/r| > 1$, where ϕ is accumulated phase per cavity transit.

In general, transient photon dynamics in resonators with input and output ports may be used to evaluate arbitrary finite sums of the form

$$\left| \sum_{n=0}^{N-1} a_n x^n \right|^2, \tag{9}$$

where complex a_n and x are determined by control pulses.

IV. COHERENT CONTROL OF MARKOVIANITY

So far, we have demonstrated that coherent photon pulses can control transient photon dynamics in a resonant cavity.
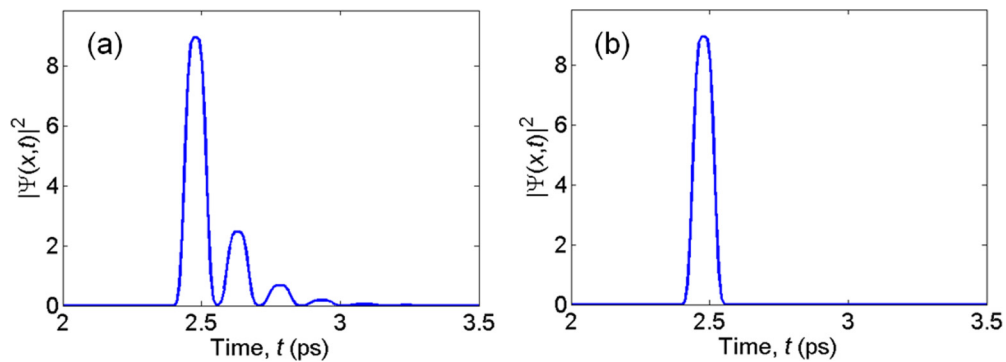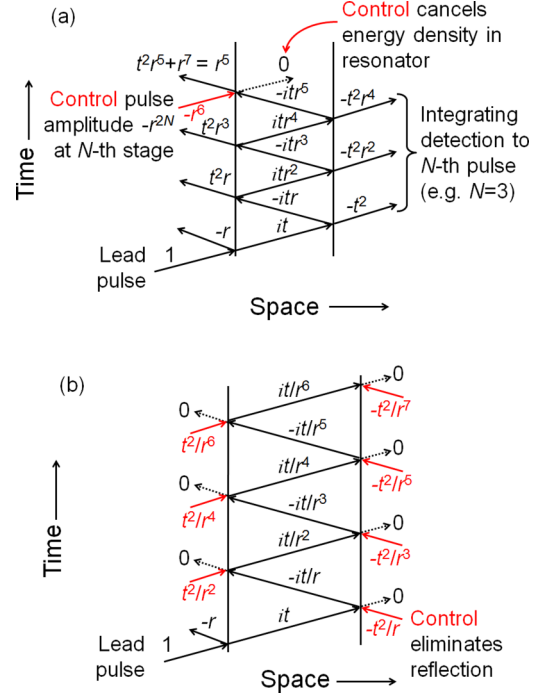

FIG. 5. (Color online) (a) Transmitted photon energy density as a function of time with no control (as in Fig. 3). (b) Same as (a), but with a control pulse to eliminate ring-down by removing all photon energy density in the cavity after exactly one round-trip time τ_{RT}. There is just one transmitted photon pulse. Photon pulse parameters are $\hbar\omega_0 = 0.827$ eV, $\hbar\Delta\omega_s = 0.207$ eV, and $T_0\omega_0 = 60$. The photon energy density scale is arbitrary.
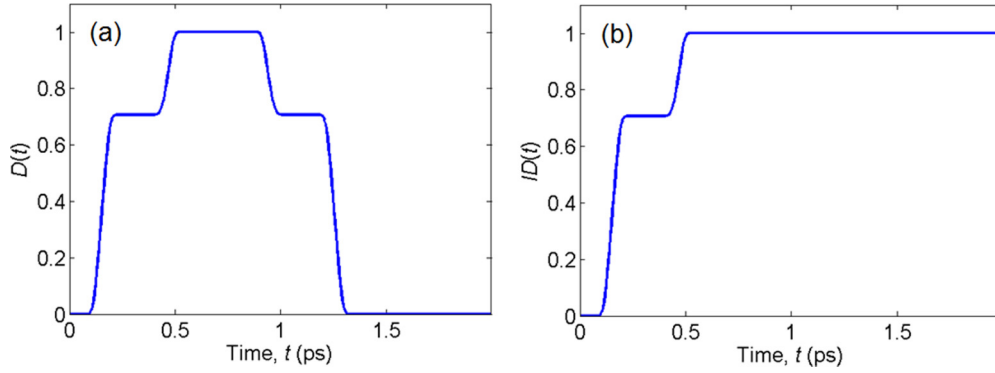
FIG. 7. (Color online) (a) Normalized measure $D(t)$ for rectangular photon pulse $\Psi_1(x,t)$ and $\Psi_2(x,t) = \Psi_1(x, t + \tau_M)$ freely propagating through spatial region A of length $L_A = 160 \times \lambda_0$. When both pulses are simultaneously in spatial region A, then $D(t) = 1$. (b) $ID(t)$, the measure of non-Markovian dynamics for the pulse in (a). Photon pulse parameters are $\hbar\omega_0 = 0.827$ eV, $\hbar\Delta\omega_s = 0.207$ eV, $T_0\omega_0 = 60$, and $\tau_M/\tau_0 = 60$.

Here we wish to show that such techniques may be understood as controlling the degree of non-Markovianity exhibited by the system. To demonstrate control of non-Markovianity in the system it is necessary to adopt a suitable measure. The definition of a proper measure of non-Markovianity is currently a topic of debate and various inequivalent definitions have been proposed [5,15–18]. These definitions suffer from the drawback of being computationally demanding, and results have been reported only for extremely simple systems consisting of a single or a few qubits. Recently, a definition of non-Markovianity valid for Gaussian states (i.e., states satisfying the Wick theorem) has been proposed which has the advantage of being computationally tractable even for high-dimensional many-body systems [19]. In practice one asks if the dynamically evolving Gaussian state under consideration is consistent with quasifree Markovian dynamics in the sense of Refs. [20–23]. The answer is no if the Hilbert-Schmidt distance $D(t) := \|\Gamma_1(t) - \Gamma_2(t)\|_{HS}$ increases for some t for initial states characterized by covariance matrices $\Gamma_{1,2}(0)$. More details on the precise definition of $D(t)$ may be found in Ref. [19]. In the following we are interested in establishing whether the exact evolution occurring in a spatial subregion A can be considered Markovian according to the Hilbert-Schmidt distance. To check this we initialize the system with two different wave packets, $\Psi_1(x,0)$ and $\Psi_2(x,0)$, which are then evolved according to the exact equation of motion to $\Psi_1(x,t)$ and $\Psi_2(x,t)$. The Hilbert-Schmidt measure $D(t)$ takes the following form [19]:

$$D(t) = \frac{1}{\sqrt{2}}\sqrt{p_{1,1}^2 + p_{2,2}^2 - 2|p_{1,2}|^2}, \qquad (10)$$

$$p_{i,j} = \int_A \Psi_i^*(x,t)\Psi_j(x,t)dx, \qquad (11)$$

where in Eq. (11) the integral is performed over region A, one of the regions under examination. The system is considered Markovian if $D(t)$ *decreases monotonically* with time for any choice of initial state. Non-Markovianity is observed when $D(t)$ increases for a pair of initial states. Instead of considering all possible initial states, we are interested in quantifying the non-Markovian content of some physically

motivated wave packets $\Psi_1(x,t)$ and $\Psi_2(x,t)$. For simplicity we choose $\Psi_2(x,t) = \Psi_1(x, t + \tau_M)$ for a fixed delay τ_M.

As an example, consider a rectangular photon pulse propagating in free space and moving from left to right. It will freely enter, propagate, and exit spatial region A. Figure 7(a) shows the resulting $D(t)$. Initially, both pulses are to the left of region A, so $D(t) = 0$. As the first pulse $\Psi_1(x,t)$ enters the region, $D(t)$ increases, eventually reaching a value of $1/\sqrt{2}$. After time delay τ_M the second pulse enters and increases $D(t)$ to its maximum value of unity, corresponding to both pulses simultaneously being in region A. There is a monotonic decrease in $D(t)$ as $\Psi_1(x,t)$ and $\Psi_2(x,t)$ leave and information leaks out of region A, indicating pure Markovian behavior.

A direct measure of non-Markovian dynamics is simply the positive contributions to $D(t)$. Defining $\sigma(t) = dD(t)/dt$, the total non-Markovian content after a time t is

$$ID(t) = \int_{\sigma(\tau) > 0 \cap [0,t]} \sigma(\tau)d\tau. \qquad (12)$$

The total non-Markovianity of the trajectories under consideration is $ID := ID(\infty)$, where a larger value of ID means more non-Markovian. Figure 7(b) shows the result of calculating $ID(t)$ for the noninteracting rectangular photon pulse considered in (a). As expected, after the two freely propagating pulses enter region A there is no further increase in $ID(t)$. The purely Markovian dynamics of a system with no scattering results in a constant value for $ID(t)$.

Photon dynamics are very different in the presence of a Fabry-Pérot resonator because energy density can be scattered and stored. Figure 8 shows the result of calculating $D(t)$ and $ID(t)$ for a rectangular photon pulse initially incident from the left in spatial regions as defined in Fig. 1(b). We ask whether the dynamics in finite-sized regions A and C can be considered Markovian and try to quantify its non-Markovianity content. Figures 8(a) and 8(c) show results for $D(t)$ and $ID(t)$ for a single initial rectangular pulse, while Figs. 8(b) and 8(d) refer to the dynamics with a control pulse applied to remove *all* photon energy density inside the resonator after just one photon round-trip time τ_{RT}, as shown in Fig. 4(b).

The functions $D(t)$ and $ID(t)$ display complex temporal patterns, some features of which can readily be connected with the physics of the resonator. For example, consider the curve
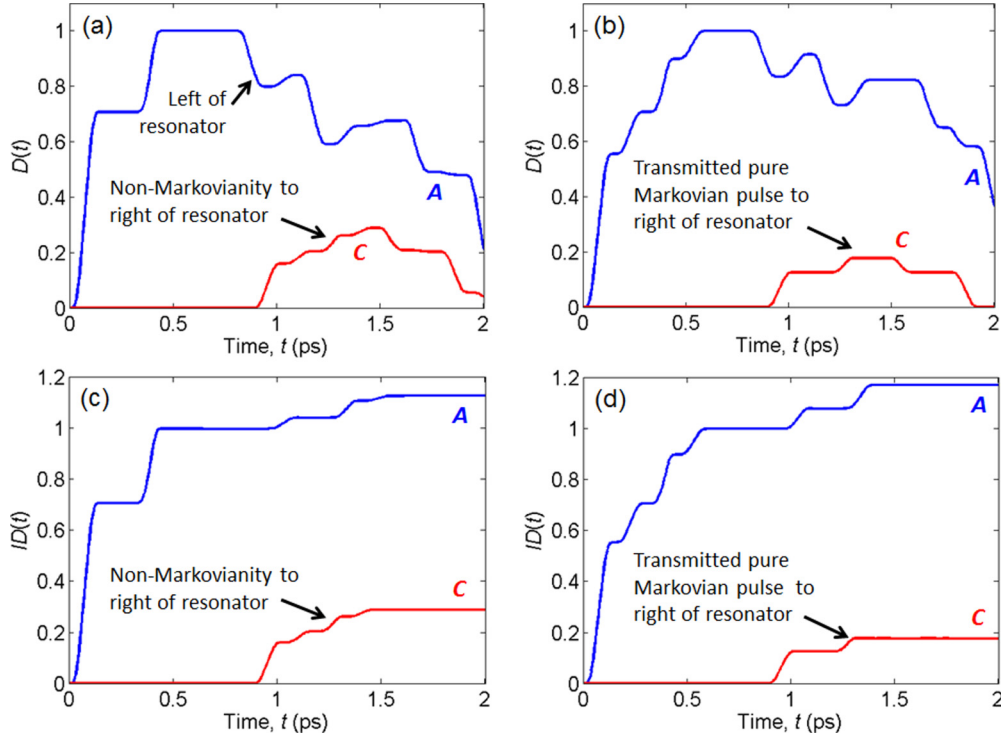
FIG. 8. (Color online) (a) $D(t)$ for rectangular photon pulse $\Psi_1(x,t)$ and $\Psi_2(x,t) = \Psi_1(x, t + \tau_M)$ in spatial region A [blue (dark gary)] to the left of the dielectric resonator and region C [red (light gray)] to the right of the resonator. $L_A = 160 \times \lambda_0$ and $L_C = 120 \times \lambda_0$. (c) $ID(t)$ for uncontrolled ring-down of $D(t)$ shown in (a). The calculated duration of non-Markovianity in region A to the left of the dielectric resonator is limited by the pulse leaving the domain. (b) $D(t)$ and (d) $ID(t)$ illustrate the use of a single control pulse to reduce non-Markovianity in transient dynamics by removing all photon energy in the resonator after exactly one cavity round-trip time τ_{RT}. Photon pulse parameters are $\hbar\omega_0 = 0.827$ eV, $\hbar\Delta\omega_s = 0.207$ eV, $T_0\omega_0 = 60$, and $\tau_M/\tau_0 = 60$.

labeled C in Fig. 8(c). Here we sent a control pulse whose effect is to eliminate completely the ring-down structure at the output (right) of the resonator. Consequently, the single transmitted pulse has a behavior identical to that for the simple dynamics illustrated in Fig. 7.

However, a simple picture seems to emerge from Fig. 8, namely, the *total* non-Markovian content of the dynamics restricted to region C (right of the resonator) diminishes after application of the control pulse. On the other hand, the total non-Markovian content restricted to region A (left of the resonator) increases in the presence of the control pulse. The sum of total non-Markovianity in regions A and C is greater for the uncontrolled case than for the controlled case.

Non-Markovianity depends on subspace size and the location to which it is referred, so this naturally provides another approach to its control. For example, evaluating $D(t)$ in region B inside the resonator involves spatial integrals over the entire cavity length L_B. However, if one evaluates $D(t)$ in a smaller portion of the cavity, then information flows in and out of that subspace as energy density builds up or decays in the resonator. Oscillatory values of $D(t)$ on a rising or falling background result, indicating non-Markovian contributions in a small subspace inside the resonator. These oscillations are averaged out when the subspace is increased to include the complete resonator cavity of length L_B (region B). This illustrates the fact that small subspaces can be *tuned* to exhibit *enhanced* non-Markovian effects.

To show how spatial placement of subspace determines Markovianity, consider a resonator with cavity length $L_B = 120 \times \lambda_0$, which defines region B, and a half space in the resonator cavity of length $L_B/2$ adjacent to the left mirror, which defines region B'. As shown in Fig. 9, in the absence of coherent control, transient photon evolution dynamics is
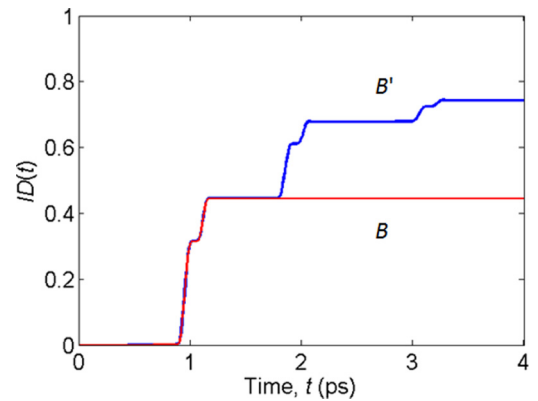

FIG. 9. (Color online) $ID(t)$ for a resonator with cavity length $L_B = 120 \times \lambda_0$, which defines region B, and a half space in the resonator cavity of length $L_B/2$ adjacent to the left mirror, which defines region B'. In the absence of a coherent control pulse, $ID(t)$ is purely Markovian for subspace B and is non-Markovian for subspace B'. Photon pulse parameters are $\hbar\omega_0 = 0.827$ eV, $\hbar\Delta\omega_s = 0.207$ eV, $T_0\omega_0 = 60$, and $\tau_M/\tau_0 = 30$.

more non-Markovian for the half-cavity subspace B' than for the full-cavity subspace B. Placing the half-cavity subspace B' symmetrically about the center of the resonator does not remove non-Markovian dynamics. This is because resonator energy density stored outside B' is reflected by the mirrors back into B', causing the non-Markovian behavior.

V. CONCLUSIONS

We have applied a Hilbert-Schmidt measure of non-Markovianity to a photon interacting with a symmetric lossless dielectric resonator. Non-Markovian transient photon dynamics in a resonator subsystem coupled to continuum states is shown to be controlled using coherent pulses. Transient photon dynamics can be controlled to within a photon-resonator transit time. The underlying physical mechanisms used to control the dynamics at resonance are conveniently described using interference arising in finite geometric series with complex amplitudes. In general, coherent pulses, combined with a suitable choice of spatial subspace, may be used to both create and control a wide range of non-Markovian transient dynamics in photon-resonator systems. This initial study has revealed a richness in both the physics and control of single-photon transient dynamics interacting with a resonator, suggesting further study is warranted.

ACKNOWLEDGMENT

APPENDIX: THE PHOTON WAVE FUNCTION

1. Introduction

To justify the use of the single-photon wave function we present a simplified version of the arguments given in Refs. [7–9,24]. This is done by first quantizing the electromagnetic field and restricting the discussion to wave propagation in one spatial dimension and lossless dielectrics. The corresponding quantized energy density operator in the dielectric is not diagonal when expressed in terms of the free-field operators. However, the energy density may be diagonalized through a unitary Bogolyubov transformation that relates the dielectric creation and annihilation operators to the free-field creation and annihilation operators. The abrupt perturbation at the air-dielectric interface may be viewed as projecting free waves onto refracted waves using the "sudden approximation." Continuity and smoothness are guaranteed via the field interface conditions.

2. The single-photon wave function in vacuum from the quantized electromagnetic field

The electromagnetic field in vacuum may be quantized in the Coulomb gauge to give

$$
\vec{A}(x^\mu) = \left(\frac{\hbar}{\epsilon_0}\right)^{1/2} \int \frac{d^3k}{(2\pi)^{3/2}} \frac{1}{\sqrt{2\omega}} \sum_{r=1}^{2} \left[\vec{\epsilon}_r(\vec{k}) a_{\vec{k},r} e^{-ik_\mu x^\mu}\right.
$$
$$
\left. + \vec{\epsilon}_r(\vec{k})^* a_{\vec{k},r}^\dagger e^{ik_\mu x^\mu}\right], \tag{A1a}
$$

$$
\vec{E}(x^\mu) = \left(\frac{\hbar}{\epsilon_0}\right)^{1/2} i \int \frac{d^3k}{(2\pi)^{3/2}} \sqrt{\frac{\omega}{2}}
$$
$$
\times \sum_{r=1}^{2} \left[\vec{\epsilon}_r(\vec{k}) a_{\vec{k},r} e^{-ik_\mu x^\mu} - \vec{\epsilon}_r(\vec{k})^* a_{\vec{k},r}^\dagger e^{ik_\mu x^\mu}\right], \tag{A1b}
$$

$$
\vec{B}(x^\mu) = \left(\frac{\hbar}{\epsilon_0}\right)^{1/2} i \int \frac{d^3k}{(2\pi)^{3/2}} \frac{1}{\sqrt{2\omega}}
$$
$$
\times \sum_{r=1}^{2} \left\{[\vec{k} \times \vec{\epsilon}_r(\vec{k})] a_{\vec{k},r} e^{-ik_\mu x^\mu}.\right.
$$
$$
\left. - [\vec{k} \times \vec{\epsilon}_r(\vec{k})^*] a_{\vec{k},r}^\dagger e^{ik_\mu x^\mu}\right\}, \tag{A1c}
$$

where $x^\mu = (ct, \vec{x})$, $k^\mu = (\omega/c, \vec{k})$, $\vec{\epsilon}_r$ is a polarization vector satisfying $\vec{k} \cdot \vec{\epsilon}_r(\vec{k}) = 0$, and $(a_{\vec{k},r}, a_{\vec{k},r}^\dagger)$ are annihilation and creation operators of a single plane-wave excitation with momentum $\vec{k}$ and polarization r satisfying

$$
[a_{\vec{k},r}, a_{\vec{k}',s}^\dagger] = \delta_{rs}\delta^{(3)}(\vec{k} - \vec{k}') . \tag{A2}
$$

The (normal-ordered) Hamiltonian and momentum are, respectively, given by

$$
:H: = \hbar \int d^3k \, \omega_k \sum_r a_{\vec{k},r}^\dagger a_{\vec{k},r} , \tag{A3}
$$

$$
:\vec{P}: = \hbar \int d^3k \, \vec{k} \sum_r a_{\vec{k},r}^\dagger a_{\vec{k},r} . \tag{A4}
$$

The vacuum $|0\rangle$ is defined by requiring $a_k|0\rangle = 0$ for all k. The one-particle state

$$
|\vec{k},r\rangle \equiv \sqrt{\frac{\omega_k}{c}} a_{\vec{k},r}^\dagger |0\rangle \tag{A5}
$$

is an eigenstate of the momentum operator with momentum $\vec{k}$ and polarization r. The reason for the $\sqrt{\omega_k}$ prefactor is that this makes the orthogonality condition given by

$$
\langle \vec{k},r|\vec{k}',r'\rangle = \frac{\omega_k}{c}\delta^{(3)}(\vec{k} - \vec{k}')\delta_{rr'} \tag{A6}
$$

Lorentz invariant [25]. The one-particle completeness condition is then given by

$$
\mathbb{1}_{1-\text{particle}} = \sum_r \int d^3k \frac{c}{\omega_k} |\vec{k},r\rangle\langle\vec{k},r| . \tag{A7}
$$

For a momentum state with $\vec{k} = k\hat{e}_z$, we can choose $\vec{\epsilon}_1 \equiv \vec{\epsilon}_+ = -(\hat{e}_x + i\hat{e}_y)/\sqrt{2}$, $\vec{\epsilon}_2 \equiv \vec{\epsilon}_- = (\hat{e}_x - i\hat{e}_y)/\sqrt{2}$, such that the momentum state satisfies

$$
:H: |k\hat{e}_z,\pm\rangle = \hbar ck|k\hat{e}_z,\pm\rangle , \tag{A8}
$$

$$
:\vec{P}: |k\hat{e}_z,\pm\rangle = \hbar k\hat{e}_z|k\hat{e}_z,\pm\rangle , \tag{A9}
$$

$$
S_z|k\hat{e}_z,\pm\rangle = \pm|k\hat{e}_z,\pm\rangle , \tag{A10}
$$

where $S_z = -i\hbar(\hat{e}_x \otimes \hat{e}_y - \hat{e}_y \otimes \hat{e}_x)$ is the z component of the angular momentum operator. Therefore, let us consider a

single-particle state $|\psi\rangle$. We define the (vector) momentum space wave function of helicity r:

$$\vec{\psi}_r(\vec{k}) = \langle \vec{k}, r | \psi \rangle . \tag{A11}$$

This is a vector due to the spin-1 nature of the photon and how the state must behave under the angular momentum operator. Furthermore, it satisfies

$$\vec{k} \cdot \vec{\psi}_r(\vec{k}) = 0 . \tag{A12}$$

The normalization of this momentum-space wave function is determined by the completeness condition:

$$1 = \langle \psi | \psi \rangle = \sum_r \int d^3k \, \frac{c}{\omega_k} \vec{\psi}_r(\vec{k})^\dagger \vec{\psi}_r(\vec{k}) . \tag{A13}$$

This normalization of the momentum-space wave function matches that defined by Ref. [7]. We define the position-space wave function $\vec{\phi}(x)$ of the state to be simply the Fourier transform of $\vec{\psi}(k)$:

$$\vec{\phi}_r(\vec{x}) = \int \frac{d^3k}{(2\pi)^{3/2}} e^{i\vec{k}\cdot\vec{x}} \vec{\psi}_r(\vec{k}) . \tag{A14}$$

This implies that

$$\langle \psi | : H : | \psi \rangle = \sum_r \int d^3x \, \vec{\phi}_r(\vec{x})^\dagger \vec{\phi}_r(\vec{x})$$
$$= \sum_r \int d^3k \, \vec{\psi}_r(\vec{k})^\dagger \vec{\psi}_r(\vec{k}) . \tag{A15}$$

Furthermore, Eq. (A15) suggests that we interpret $\vec{\psi}_r(\vec{k})^\dagger \vec{\psi}_r(\vec{k})d^3k$ as the energy density in shell $\vec{k}$ and $\vec{k} + d\vec{k}$ in momentum space rather than a probability density [9]. Finally, we note that

$$\langle \vec{k}, \sigma | : H : | \psi \rangle = c\hbar |\vec{k}| \vec{\psi}_\sigma(\vec{k})$$
$$= c\hbar \sigma (\vec{s} \cdot \vec{k}) \vec{\psi}_\sigma(\vec{k})$$
$$= ic\hbar \sigma \vec{k} \times \vec{\psi}_\sigma(\vec{k}), \tag{A16}$$

where $\vec{s} = (s_x, s_y, s_z)$ are the three spin-1 matrices (generators of rotations for spin-1 particles; angular momentum is $\vec{S} = \hbar\vec{s}$), and we use the feature of spin-1 matrices that $\vec{a} \times \vec{b} = -i(\vec{a} \cdot \vec{s})\vec{b}$ [9]. Since the Hamiltonian is the generator of time translations, we have our Schrödinger equation,

$$i\hbar \partial_t \vec{\psi}_\sigma(\vec{k}, t) = ic\hbar \sigma \vec{k} \times \vec{\psi}_\sigma(\vec{k}, t) , \tag{A17}$$

or in position space,

$$i\hbar \partial_t \vec{\phi}_\sigma(\vec{x}, t) = c\hbar \sigma \nabla \times \vec{\phi}_\sigma(\vec{x}, t) . \tag{A18}$$

Applying another $i\hbar\partial_t$, we recover the Helmholtz equation:

$$-\partial_t^2 \vec{\phi}_\sigma(\vec{x}, t) = c\nabla \times [c\nabla \times \vec{\phi}_\sigma(\vec{x}, t)] = -c^2 \nabla^2 \vec{\phi}_\sigma(\vec{x}, t) , \tag{A19}$$

where in the last equality we used Eq. (A12).

3. Quantization in a linear lossless dielectric

One way to study the effect of the presence of the lossless linear medium is to consider the modified Hamiltonian density [24]

$$\mathcal{H} = \frac{1}{2}\left(\epsilon_0 \vec{E}^2 + \frac{1}{\mu_0}\vec{B}^2 + \chi \vec{E}^2\right) . \tag{A20}$$

(For other methods see Ref. [26].) Inserting the quantized fields in vacuum into this expression clearly shows that the Hamiltonian density operator is not diagonal in terms of the free-field creation and annihilation operators $(a_{\vec{k},\sigma}^\dagger, a_{\vec{k},\sigma})$. Nevertheless, the Hamiltonian density can be diagonalized in terms of "refracted-wave" operators $(b_{\vec{k},\sigma}^\dagger, b_{\vec{k},\sigma})$ via a Bogolyubov transformation [24]. In this basis, the Hamiltonian density has the same eigenvalues as in vacuum, but the momentum operator is renormalized by a factor of the index of refraction, such that the results match the known results from classical optics.

At an abrupt vacuum-dielectric interface, where the permittivity changes from $\epsilon = \epsilon_0$ to $\epsilon = \sqrt{n_r}\epsilon_0$, we can treat the change in the momentum operator (from the vacuum form to the renormalized form) in the "sudden approximation" [24]. For example, a single excitation $a_{\vec{k},\sigma}^{\dagger,\sigma}|0\rangle$ gets projected to [24]

$$\left(\frac{2\sqrt{n_r}}{n_r + 1} b_{\vec{k},\sigma}^\dagger + \frac{n_r - 1}{n_r + 1} a_{\vec{k},\sigma}^\dagger\right)|0\rangle, \tag{A21}$$

such that the probability of reflection and transmission agrees with the classical result for energy reflection and transmission. With these results in mind, we can generalize our equation for the single-photon wave function to satisfy the Helmholtz equation in the presence of a lossless dielectric:

$$\nabla \times \left(\frac{1}{\mu(x)}\nabla \times \vec{\psi}_\sigma(\vec{x}, t)\right) = -\epsilon(x)\partial_t^2 \vec{\psi}_\sigma(\vec{x}, t) . \tag{A22}$$

For a linearly polarized, transverse field which propagates in the x direction one has $\vec{\psi}_\sigma(\vec{x}, t) = (0, \phi_\sigma(x, t), 0)$, and one recovers Eq. (3) after a time Fourier transform.

[1] A. Yariv, Y. Xu, R. K. Lee, and A. Scherer, Opt. Lett. **24**, 711 (1999).

[2] E. E. Hach, A. W. Elshaari, and S. F. Preble, Phys. Rev. A **82**, 063839 (2010).

[3] I. M. Mirza, S. J. van Enk, and H. J. Kimble, J. Opt. Soc. Am. B **30**, 2640 (2013).

[4] J.-T. Shen and S. Fan, Phys. Rev. A **79**, 023837 (2009).

[5] H.-P. Breuer, E.-M. Laine, and J. Piilo, Phys. Rev. Lett. **103**, 210401 (2009).

[6] B. Bylicka, D. Chruściński, and S. Maniscalco, Sci. Rep **4**, 5720 (2014).

[7] I. Bialynicki-Birula, Acta Phys. Pol. **86**, 97 (1994).

[8] J. E. Sipe, Phys. Rev. A **52**, 1875 (1995).

[9] B. J. Smith and M. G. Raymer, New J. Phys. **9**, 414 (2007).

[10] E. O. Kane, in *Tunneling Phenomena in Solids*, edited by E. Burstein and S. Lundqvist (Springer, New York, 1969), pp. 1–11.

[11] A. Levi, *Applied Quantum Mechanics* (Cambridge University Press, Cambridge, 2014).

[12] M. Born, E. Wolf, A. Bhatia, P. Clemmow, D. Gabor, A. Stokes, A. Taylor, P. Wayman, and W. Wilcock, *Principles of Optics: Electromagnetic Theory of Propagation, Interference and Diffraction of Light* (Cambridge University Press, Cambridge, 1999).

[13] B. Saleh and M. Teich, *Fundamentals of Photonics*, Wiley Series in Pure and Applied Optics (Wiley, Hoboken, NJ, 2013).

[14] J. O'Gorman, A. F. J. Levi, D. Coblentz, T. Tanbun-Ek, and R. A. Logan, Appl. Phys. Lett. **61**, 889 (1992).

[15] D. Chruściński and A. Kossakowski, Phys. Rev. Lett. **104**, 070406 (2010).

[16] A. Rivas, S. F. Huelga, and M. B. Plenio, Phys. Rev. Lett. **105**, 050403 (2010).

[17] D. Chruściński, A. Kossakowski, and A. Rivas, Phys. Rev. A **83**, 052128 (2011).

[18] Á. Rivas, S. F. Huelga, and M. B. Plenio, arXiv:1405.0303.

[19] N. Chancellor, C. Petri, L. Campos Venuti, A. F. J. Levi, and S. Haas, Phys. Rev. A **89**, 052119 (2014).

[20] T. Prosen, New J. Phys. **10**, 043026 (2008).

[21] T. Prosen and T. H. Seligman, J. Phys. A **43**, 392004 (2010).

[22] T. Prosen, J. Stat. Mech. (2010) P07020.

[23] J. Eisert and T. Prosen, arXiv:1012.5013.

[24] I. Abram, Phys. Rev. A **35**, 4661 (1987).

[25] M. Peskin and D. Schroeder, *An Introduction to Quantum Field Theory*, Advanced Book Classics (Westview Press, Boulder, CO, 1995).

[26] R. J. Glauber and M. Lewenstein, Phys. Rev. A **43**, 467 (1991).